Ceramics International 51 (2025) 6968–6975

Contents lists available at ScienceDirect

Ceramics International

journal homepage: www.elsevier.com/locate/ceramint

Preparation and properties of high-entropy rare earth niobate $LnNbO_4$ microwave dielectric ceramics

Xinrong Yang [a,b,1], Deqin Chen [a,1], Guobin Zhu [a], Siyu Xiong [a], Xiaowei Zhu [a], Laijun Liu [a], Chunchun Li [a,c,*]

[a] Guangxi University Key Laboratory of Non-ferrous Metal Oxide Electronic Functional Materials and Devices, College of Material Science and Engineering, Guilin University of Technology, Guilin, 541004, China
[b] CAS Key Laboratory of Materials for Energy Conversion and Department of Materials Science and Engineering, University of Science and Technology of China, No. 96 Jinzhai Rd, Anhui, Hefei, 230026, China
[c] Guangxi Key Laboratory of Embedded Technology and Intelligent System, Guilin University of Technology, Guilin, 541004, China

ARTICLE INFO

Handling Editor: Dr P. Vincenzini

Keywords:
Microwave dielectric properties
High-entropy strategy
Rare earth lanthanum niobate
Ceramics

ABSTRACT

The impact of configurational entropy on the microwave dielectric properties of $LnNbO_4$ fergusonite was investigated by designing a series of high-entropy counterparts, including (La, Nd, Sm, Ho, Yb, Y)NbO_4 (6RNO), (La, Nd, Sm, Eu, Ho, Yb, Y)NbO_4 (7RNO), (La, Nd, Sm, Eu, Gd, Ho, Yb, Y)NbO_4 (8RNO), and (La, Nd, Sm, Eu, Gd, Ho, Tm, Yb, Lu, Y)NbO_4 (10RNO). Simply prepared by the solid-state route, a pure phase with a monoclinic fergusonite structure of space group $C/2c$ was obtained. By comparing the microstructural evolution and lattice vibration modes, an analysis was conducted on the variations in microwave dielectric performances. It was confirmed that the permittivity (ε_r) is primarily influenced by relative density, while the quality factor ($Q \times f$) exhibits a strong correlation with packing fraction and lattice vibrations. The resonant frequency temperature coefficient (τ_f) is significantly associated with bond valence. The optimal microwave dielectric properties were achieved in 7RNO ceramics at a temperature of 1270 °C, resulting in a relative density of 95.43 %. The microwave dielectric properties were measured as $\varepsilon_r = 18.62$, $Q \times f = 35200$ GHz, $\tau_f = -23.28$ ppm/°C. The present study expands the application of entropy engineering to achieve ultrahigh configurational entropy in microwave dielectric ceramics. These findings demonstrate that optimizing the configuration entropy is an effective approach for manipulating the dielectric properties, thereby providing valuable insights for material component design.

1. Introduction

The high-entropy materials are characterized by the presence of multiple components occupying one or more Wyckoff sites in their solid solutions [1]. The high values of configurational entropy (ΔS_{conf}) counteract the enthalpy effect among multiple principal elements, thereby resulting in a reduction in the Gibbs free energy (ΔG), which is defined as the difference between the enthalpy (ΔH) and temperature multiplied by entropy change ($T\Delta S$). This reduction in Gibbs free energy enhances the stability of the high-entropy material system, expanding its potential for material design and offering a novel approach to developing new materials.

The configurational entropy of the system can be calculated according to Eq. (1):

$$\Delta S_{conf} = -R\sum_{i}^{n} x_i \ln x_i \quad (1)$$

where R is the gas constant in the ideal state, n is the number of components, and x_i is the concentration of the ith component. The configurational entropy is influenced by the quantity and concentration of each individual component. Based on the magnitude of the ΔS_{conf} value, the system is normally classified as low entropy ($\Delta S_{conf} \leq 1.0R$), medium entropy ($1.0R < \Delta S_{conf} < 1.5R$), and high-entropy ($\Delta S_{conf} \geq 1.5R$) [2]. In 2015, Rost et al. [3] extended the study of high-entropy materials to

* Corresponding author. Guangxi University Key Laboratory of Non-ferrous Metal Oxide Electronic Functional Materials and Devices, College of Material Science and Engineering, Guilin University of Technology, Guilin, 541004, China.
E-mail address: lichunchun2003@126.com (C. Li).
[1] Xinrong Yang and Deqin Chen contributed equally to this work.

https://doi.org/10.1016/j.ceramint.2024.12.131
Received 12 November 2024; Received in revised form 2 December 2024; Accepted 9 December 2024
Available online 9 December 2024

ceramics, firstly proposed high-entropy ceramics ($Mg_{0.2}Co_{0.2}Ni_{0.2}Cu_{0.2}Zn_{0.2}$)O by solid-state synthesis. Subsequently, "high-entropy" was extended to ceramic materials such as carbides, borides, silicides, fluorides, etc [4–7]. High-entropy ceramics adopt the identical high-entropy strategy as high-entropy alloys. The high-entropy strategy provides abundant feasibility for material design and property optimization [8–10].

Recently, high-entropy strategies have been introduced into the design of microwave dielectric materials to improve dielectric properties. For example, Xiang et al. [11] proposed Li($Gd_{0.2}Ho_{0.2}Er_{0.2}Yb_{0.2}Lu_{0.2}$)$GeO_4$ high-entropy ceramics with an olivine structure, which exhibit exceptional microwave dielectric characteristics ($\varepsilon_r = 7.6$, $Q \times f = 11700$ GHz, and $\tau_f = -7.4$ ppm/°C). Moreover, the high-entropy strategy was also employed in a series of microwave dielectric materials, e.g., ($Mg_{0.2}Ni_{0.2}Zn_{0.2}Co_{0.2}Mn_{0.2}$)$_2SiO_4$, ($Mg_{0.2}Co_{0.2}Ni_{0.2}Li_{0.2}Zn_{0.2}$)$Al_2O_4$, ($Zn_{1/6}Ba_{1/6}Ca_{1/6}Sr_{1/6}La_{1/3}$)$Ti_{1-x}Al_xO_3$ ($0 \le x \le 0.1$), and ($La_{0.2}Nd_{0.2}Sm_{0.2}Eu_{0.2}Gd_{0.2}$)$_2Zr_3(MoO_4)_9$ (L_5ZMO) [12–15], demonstrating its effectiveness in optimizing dielectric properties. In our previous work, medium- and high-entropy $LnNbO_4$ ceramics was investigated, where three, four, and five rare earth elements were co-occupied in the Ln-site. The results demonstrated an improvement in ε_r and $Q \times f$ as the configurational entropy increased, and the τ_f value was effectively adjusted from a significantly negative value to a reduced level [16]. This unexpected finding highlights the potential of entropy engineering for regulating microwave dielectric properties of $LnNbO_4$ ceramics. Thus, the question arises as to whether the dielectric properties can be further enhanced (improved $Q \times f$ value and suppressed τ_f value) by increasing the configuration entropy, or if there exists an optimal configuration entropy that corresponds to the optimal dielectric properties.

To address the question, configuration entropy was further increased through compositional design in $LnNbO_4$ ceramics by augmenting the number of rare earth elements in the Ln-site, resulting in the formation of ultrahigh-entropy ceramics such as ($La_{1/6}Nd_{1/6}Sm_{1/6}Ho_{1/6}Yb_{1/6}Y_{1/6}$)$NbO_4$ (6RNO, $\Delta S_{conf} = 1.792$R), ($La_{1/7}Nd_{1/7}Sm_{1/7}Eu_{1/7}Ho_{1/7}Yb_{1/7}Y_{1/7}$)$NbO_4$ (7RNO, $\Delta S_{conf} = 1.946$R), ($La_{1/8}Nd_{1/8}Sm_{1/8}Eu_{1/8}Gd_{1/8}Ho_{1/8}Yb_{1/8}Y_{1/8}$)$NbO_4$ (8RNO, $\Delta S_{conf} = 2.079$R) and ($La_{1/10}Nd_{1/10}Sm_{1/10}Eu_{1/10}Gd_{1/10}Ho_{1/10}Tm_{1/10}Yb_{1/10}Lu_{1/10}Y_{1/10}$)$NbO_4$ (10RNO, $\Delta S_{conf} = 2.303$R). The influence of configuration entropy on the crystal structure and microwave dielectric properties of $LnNbO_4$ ceramics was further investigated.

2. Experimental procedures

The solid-state reaction method was utilized for synthesizing 6RNO, 7RNO, 8RNO, and 10RNO utilizing high-purity oxides: La_2O_3、Nd_2O_3、Sm_2O_3、Eu_2O_3、Gd_2O_3、Ho_2O_3、Tm_2O_3、Yb_2O_3、Lu_2O_3、Y_2O_3、Nb_2O_5 (≥99.9 %, Aladdin). The raw materials were accurately weighed and thoroughly mixed by ball milling for 6 h using alcohol as the medium. The dried powder was then calcined at 1250 °C for 8 h. After that, the pre-fired powder underwent another round of ball milling for 6 h. A small amount of polyvinyl alcohol (PVA, 5 wt%) was added for granulation, and the powder was pressed into cylindrical samples with dimensions of Φ 12 mm × 7 mm under a pressure of 70 MPa. The ceramic samples were heated to remove the PVA at 550 °C for 6 h and finally sintered at temperatures ranging from 1210 °C to 1290 °C for 4 h.

X-ray diffraction (XRD; Empyrean, PANalytical, Netherlands) was employed for the analysis of the phase formation and purity of the samples. The microscopic morphology was examined using scanning electron microscopy (SEM; S-4800, Hitachi High-Technologies, Japan), Prior to testing, the samples were polished and subsequently coated with double-sided conductive adhesive on the unpolished side to prevent charge accumulation on the ceramic surface. The particle size and distribution were analyzed using Nano Measurer. The transmission electron microscopy (TEM; JEM-2100F, JEOL, Japan) provided detailed insights into the lattice features. Local structural characteristics were assessed through Raman spectroscopy (Raman; Fisher DXR, Thermo Electron, USA). The bulk density of the ceramic samples was determined using the Archimedes drainage method. The theoretical density (ρ_{theory}) of ceramics was computed from the mass and volume of the unit cell. A microwave vector network analyzer (Keysight E5071C, Keysight Technologies, USA) was utilized to measure the microwave dielectric properties and calculate the temperature coefficient of resonance frequency (τ_f) according to Eq. (2).

$$\tau_f = \frac{f_{85} - f_{25}}{f_{25}(T_{85} - T_{25})} \quad (2)$$

where f_{85} and f_{25} are the resonant frequencies of the sample when the temperature of the thermostat is 25 °C and 85 °C, respectively.

3. Results and discussion

3.1. Sintering behavior and microscopic characterization

The bulk density of $LnNbO_4$ ceramics sintered at temperatures ranging from 1210 to 1290 °C is shown in Fig. 1 It is closely related to the sintering temperature. Prior to reaching their peak values, the bulk density increases steadily with sintering temperatures due to enhanced internal grain growth. All four components achieved their maximum bulk density at 1270 °C. However, when the sintering temperature exceeds 1270 °C, the bulk density decreases, due to abnormal grain growth. Therefore, it can be concluded that the optimal sintering temperature is 1270 °C. The relative densities of 6RNO, 7RNO, 8RNO, and 10RNO ceramics were measured to be 98.17 %, 95.43 %, 96.23 %, and 96.49 % respectively. All the obtained results exceed 95 %, indicating that these ceramic samples are suitable for subsequent characterizations of their structural and dielectric properties.

Fig. 2(a–d) presents the SEM images of 6RNO, 7RNO, 8RNO, and 10RNO ceramics sintered at 1270 °C. All compositions exhibit favorable grain boundaries and grain growth, characterized by uniform grain size, compact grain packing and minimal porosity, indicating effective densification. The average grain size was calculated for all samples sintered at 1270 °C for 4 h to characterize their grain growth. Further, the grain sizes of $LnNbO_4$ ceramics for different components, as illustrated in Fig. 3, are predominantly concentrated within the range of 1.5–3.5 μm. As the number of Ln element types increases, there is an initial increase followed by a subsequent decrease in the average grain size. The SEM-EDS results for 7RNO ceramics sintered at 1270 °C are shown in Fig. 2 (e), indicating a uniform distribution of all elements without any signs of enrichment, further confirming the successful solid

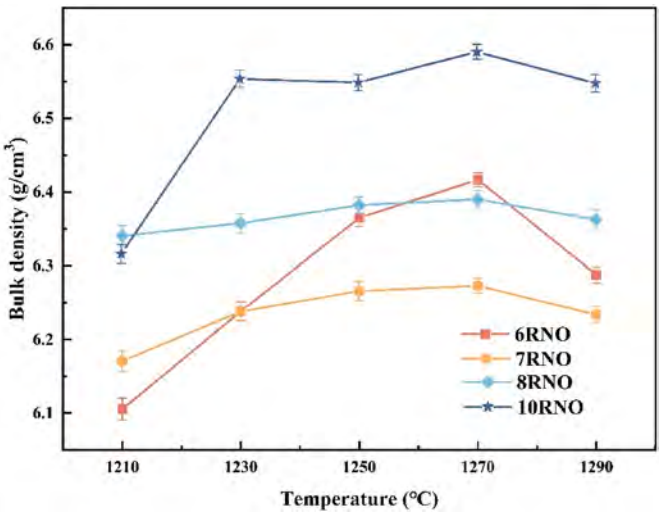

Fig. 1. Bulk density of $LnNbO_4$ ceramics at 1210–1290 °C.

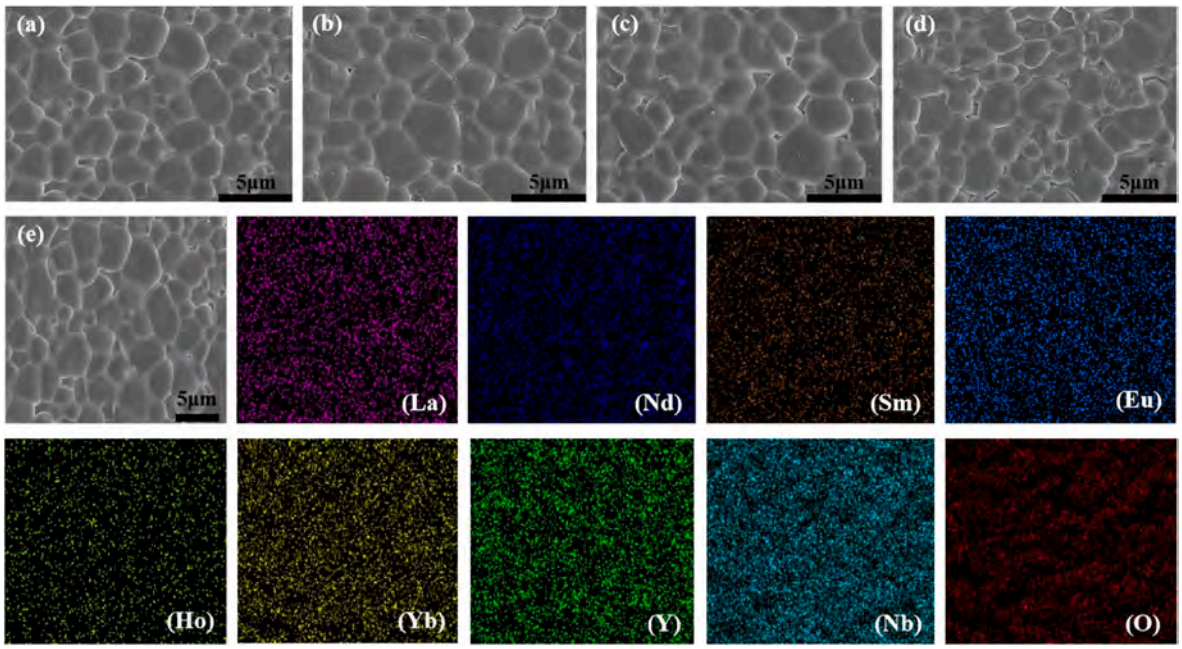

Fig. 2. SEM of (a) 6RNO, (b) 7RNO, (c) 8RNO, and (d) 10RNO ceramics at 1270 °C sintering temperature; (e) SEM-EDS of 7RNO ceramics sintered at 1270 °C, the elements in different colors are La, Nd, Sm, Eu, Ho, Yb, Y, Nb, O, respectively. (For interpretation of the references to color in this figure legend, the reader is referred to the Web version of this article.)

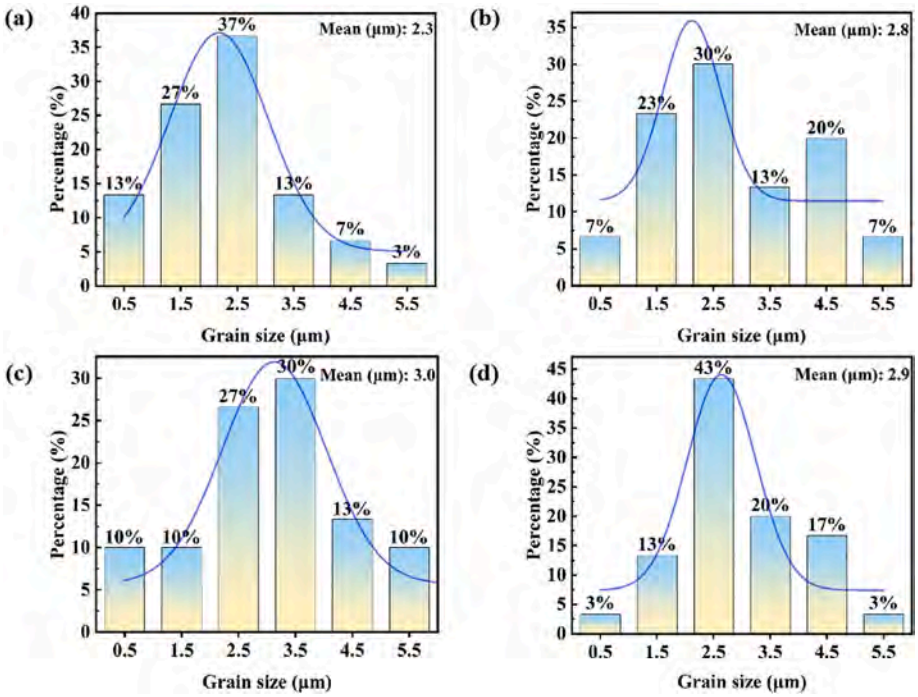

Fig. 3. The grain size distribution of (a) 6RNO, (b) 7RNO, (c) 8RNO, and (d) 10RNO ceramics at 1270 °C, and the normal distribution is used as a function to fit the grain size distribution.

solution of multiple ions, a testament to the high-entropy effect that enhances compositional homogeneity in the ceramics.

3.2. Phase characterizations

The XRD patterns of high-entropy $LnNbO_4$ ceramics sintered at 1270 °C for 4 h are presented in Fig. 4 (a). A comparison with the standard PDF cards reveals that the distribution of diffraction peaks closely matches with $NdNbO_4$ (PDF# 96-152-5403), which is characterized by a monoclinic fergusonite structure belonging to a *C*2/*c* space group. The crystal structure of 8RNO ceramics is illustrated in Fig. 4 (b). Within this structure, La^{3+}, Nd^{3+}, Sm^{3+}, Eu^{3+}, Gd^{3+}, Ho^{3+}, Yb^{3+} and Y^{3+} equally and randomly occupy the Ln-site [17]. It is constituted by $[NbO_4]$ tetrahedra and $[LnO_8]$ decahedra, in which the adjacent $[LnO_8]$ decahedra units form chains via edge-sharing and $[NbO_4]$ and $[LnO_8]$ are corner-connected by sharing oxygen ions. Importantly, no additional

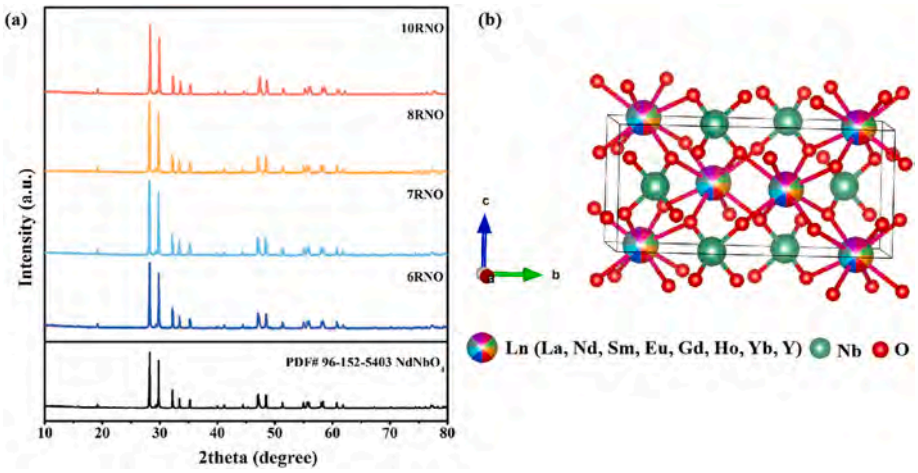

Fig. 4. (a) XRD patterns of $LnNbO_4$ ceramics sintered at 1270 °C, (b) the crystal structure of 8RNO ceramics.

secondary phase peaks were observed in the XRD patterns of the high-entropy $LnNbO_4$, indicating that multiple elements have successfully incorporated into the $LnNbO_4$ ceramics, highlighting the effectiveness of the high-entropy approach in achieving a single-phase structure.

To further confirm the crystal structure of $LnNbO_4$, the monoclinic fergusonite structure was selected as the refinement model. Lattice parameters were obtained from Rietveld refinements of the XRD patterns, as shown in Fig. 5, with the measured XRD values showing excellent correspond with the fitted values. Table 1 lists the refinement parameters for the $LnNbO_4$ ceramics, where the goodness-of-fit factors R_p and R_{wp}, are both below 10 %, indicating the excellence and reliability of the refinement fitting. Table 2 provides the effective radius ionic radius in the Ln-site. Notably, the cell volume (V_{cell}) of the $LnNbO_4$ ceramics exhibits a progressive decrease as from 6RNO to 10RNO the Ln-site ion radius decreases, demonstrating the multi-ion solid solution's efficacy in modulating the crystal structures.

As illustrated in Fig. 6, extensive microstructural information about 7RNO and 10RNO ceramic bulks via selected-area electron diffraction (SAED) and high-resolution transmission electron microscopy (HRTEM). The bright and well-ordered diffraction spots in the SAED patterns of both ceramics, as seen in Fig. 6 (a) for 7RNO along the [1–10] crystal axis, and 10RNO along the [111] crystal axis in Fig. 6 (c) suggest a high degree of crystallinity. The SAED patterns can be indexed to the diffraction spots corresponding to the (222), (220), and (002) planes for 7RNO, and the (0–11), (1–10), and (10–1) planes for 10RNO, respectively. HRTEM images in Fig. 6 (b) and 6 (d) reveal the crystal plane spacing for the (200) plane in 7RNO and 0.489 nm for the (110) plane in 10RNO ceramics, corroborating monoclinic structure (space group: $C2/c$) as determined by X-ray diffraction (XRD) results. The uniform distributed of elements at the nanometer, as presented in the TEM-EDS diagram of the 7RNO ceramics in Fig. 6 (e) which corroborates the

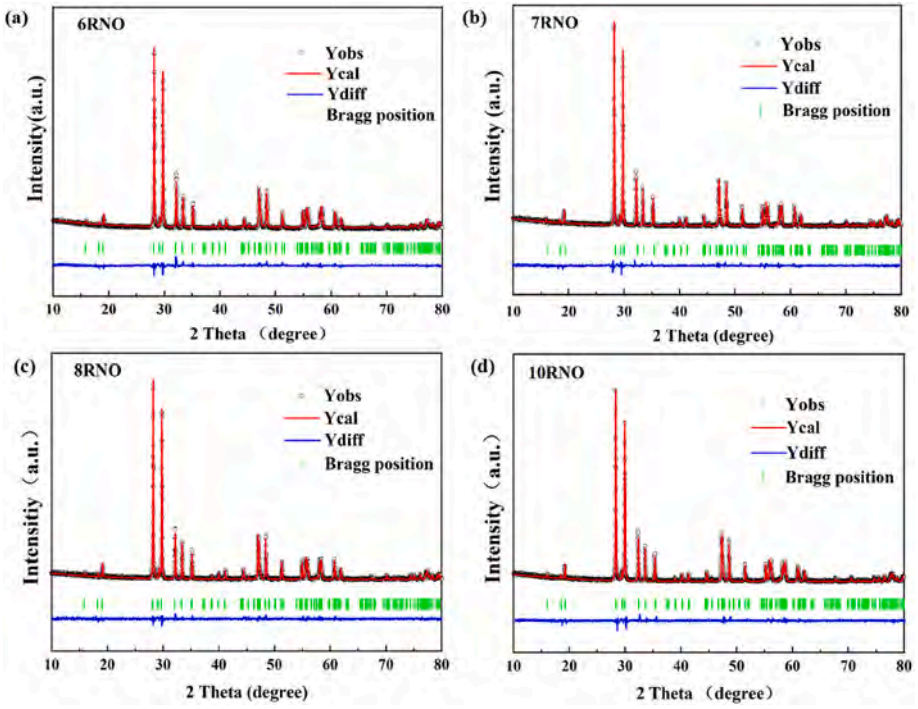

Fig. 5. (a–d) Rietveld refinement of XRD patterns for $LnNbO_4$ ceramics, the black circles represent the sample XRD test data, the red solid lines represent the model fitting data, the green vertical lines represent the Bragg diffraction position, and the blue solid lines represent the error value between the measured value and the fitted value. (For interpretation of the references to color in this figure legend, the reader is referred to the Web version of this article.)

Table 1
XRD refinement parameters of $LnNbO_4$ ceramics sintered at 1270 °C.

sample	a (Å)	b (Å)	c (Å)	V_{cell} (Å^3)	R_p (%)	R_{wp} (%)	χ^2	ρ_{th} (g/cm^3)
6RNO	5.3806 (9)	11.1230 (6)	5.1127 (4)	305.0880	6.58	8.35	1.60	6.54
7RNO	5.3814 (2)	11.1215 (4)	5.1119 (4)	305.0260	5.89	7.56	1.44	6.57
8RNO	5.3798 (8)	11.1173 (0)	5.1108 (6)	304.7510	5.41	6.94	1.33	6.64
10RNO	5.3524 (4)	11.0647 (4)	5.0983 (6)	301.0300	5.74	7.31	1.40	6.83

Table 2
Effective ionic radius in the Ln-site [18].

element	Coordination Number	R^e (Å)	element	Coordination Number	R^e (Å)
La^{3+}	8	1.16	Ho^{3+}	8	1.015
Nd^{3+}	8	1.09	Tm^{3+}	8	0.994
Sm^{3+}	8	1.079	Yb^{3+}	8	0.985
Eu^{3+}	8	1.066	Lu^{3+}	8	0.977
Gd^{3+}	8	1.053	Y^{3+}	8	1.019

SEM-EDS findings and reaffirms the successful solid solution of multiple ions. These findings collectively affirm the structural integrity and homogeneity of $LnNbO_4$ ceramics.

Raman spectroscopy can provide vibration characteristics of chemical bonds and functional groups, which is helpful to further study and analyze the microstructure of $LnNbO_4$ ceramics. Fig. 7 (a) presents the Raman spectrum with Gauss-Lorentz fitting results. Each characteristic peak in the Raman spectrum of $LnNbO_4$ ceramics corresponds to distinct vibration modes. Theoretically, monoclinic $LnNbO_4$ possesses 18 Raman-active vibration modes [19], which can be expressed as:

$$\Gamma = 8A_g + 10B_g \tag{3}$$

Due to deviations from the symmetry of the space group or accidental simplicity, 15, 17, 17, and 9 Raman-active vibrational modes were detected for the 6RNO, 7RNO, 8RNO, and 10RNO ceramics, respectively. Vibrations below 300 cm^{-1} are associated with the [NbO_4] stacking modes [20]. The characteristic peaks in the range of 300 cm^{-1} to 1000 cm^{-1} primarily correspond to the Nb-O bond vibrations. Symmetric stretching vibrations of the Nb-O bonds are represented by modes near 320 cm^{-1} and 810 cm^{-1}, while antisymmetric vibrational modes of the Nb-O bonds are observed in the ranges of 400 cm^{-1} to 500 cm^{-1} and 600 cm^{-1} to 700 cm^{-1} [21,22]. The variations in the Raman shift are indicative of changes in interatomic forces and lattice distortions. Fig. 7 (b) illustrates the amplified Raman peaks around 320 cm^{-1} and 810 cm^{-1}, with the full width at half maximum (FWHM) values indicated. As the configurational entropy of $LnNbO_4$ ceramics increases, the FWHM of the Raman peaks near 320 cm^{-1} and 810 cm^{-1} tends to widen. The broadening of these Raman characteristic peaks suggests that diffusion vibrational modes emerge with increasing disorder, a phenomenon also reflected in the abnormally broadened Raman peaks of the 10RNO sample, which has an exceptionally high-entropy value. These findings demonstrate that entropy stabilization effects can be achieved in pure-phase $LnNbO_4$ ceramics.

3.3. Microwave dielectric properties

Fig. 8 (a) illustrates the variation of relative permittivity (ε_r) with sintering temperature for $LnNbO_4$. The ε_r values for the four components range from 17 to 20. The ε_r of each component initially increases with rising sintering temperature until it exceeds 1270 °C, after which a decreasing trend in permittivity is observed. The trends in permittivity

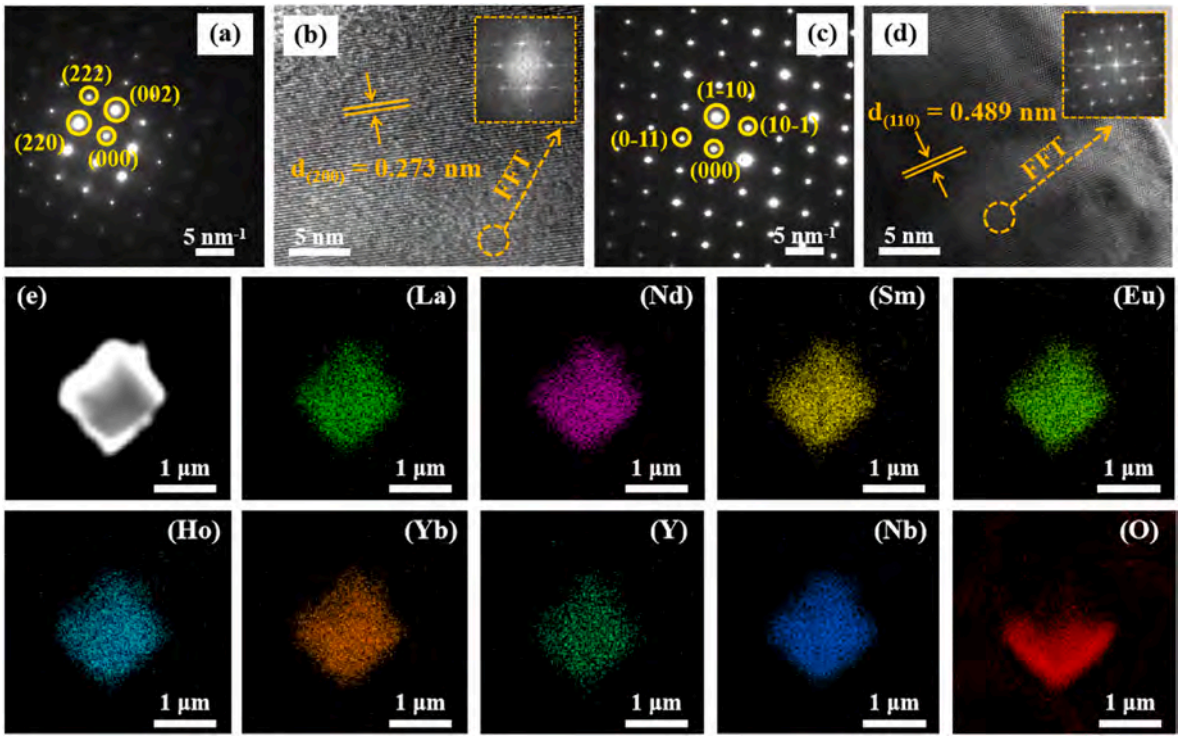

Fig. 6. (a) SAED of 7RNO ceramics along [1–10]; (b) HRTEM of 7RNO ceramics along (200); (c) SAED of 10RNO ceramics along [111]; (d) HRTEM of 10RNO ceramics along (110); (e) TEM-EDS mapping of 7RNO, the elements in different colors are La, Nd, Sm, Eu, Ho, Yb, Y, Nb, O, respectively. (For interpretation of the references to color in this figure legend, the reader is referred to the Web version of this article.)

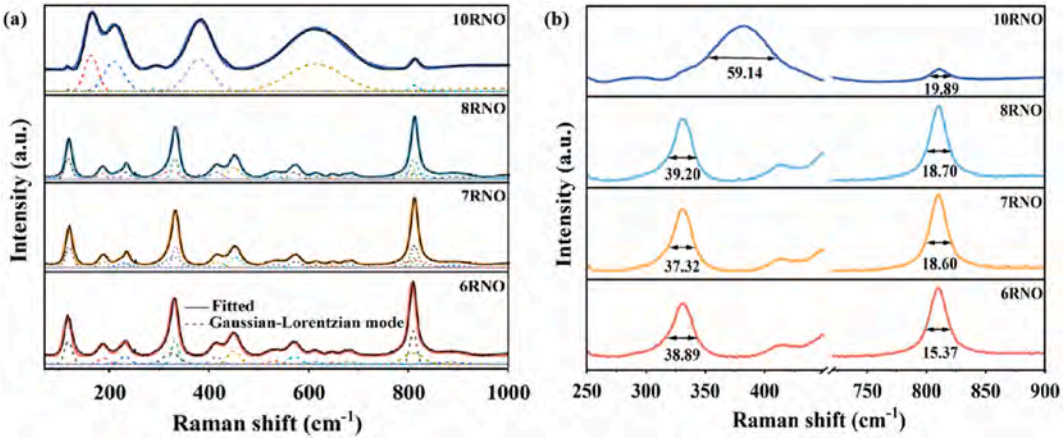

Fig. 7. (a) Raman spectra of $LnNbO_4$ ceramics; (b) Amplified Raman spectra at 320 and 810 cm^{-1} and their FWHM.

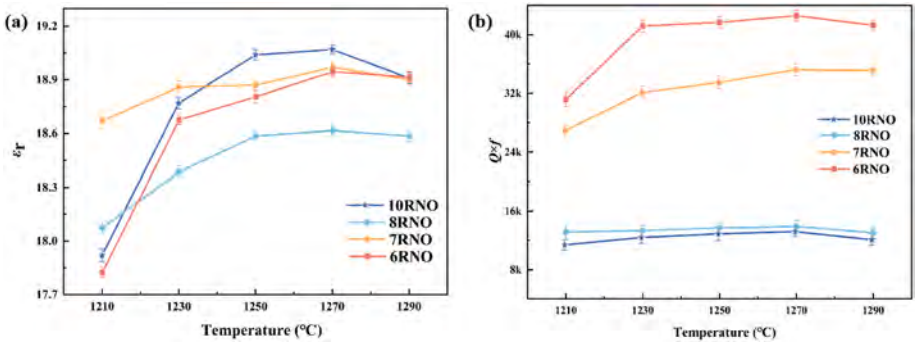

Fig. 8. (a) Relative permittivity, (b) quality factor of $LnNbO_4$ ceramics as a function of sintering temperature.

and density are generally similar, indicating that density plays a crucial role in regulating the relative permittivity of ceramics.

Additionally, ionic polarizability significantly contributes to the relative permittivity at microwave frequencies. The Clausius–Mosotti (C–M) equation (Eq. (4)) effectively correlates the relative permittivity, supporting the relationship of α/V_m as a whole. Generally, relative permittivity is proportional to the ionic polarizability per unit volume (α/V_m). As shown in Table 3, the measured ε_r values of four components sintered at 1270 °C are 18.95, 18.97, 18.62, and 19.07, respectively. The ε_r of 10RNO ceramics (19.07) is higher than that of the other ceramics, which can be attributed to the greater α/V_m value of 10RNO ceramics. It is noteworthy that 6RNO and 8RNO ceramics have the same α/V_m values; however, there is a difference in ε_r. This discrepancy arises because 6RNO ceramics possess a higher relative density than 8RNO ceramics, and the elevated ε_r values result from a synergistic effect of $\rho_{relative}$ and α/V_m.

$$\varepsilon_{th}=\frac{3V_m+8\pi\alpha}{3V_m-4\pi\alpha}=\frac{3+8\pi\alpha/V_m}{3-4\pi\alpha/V_m} \quad (4)$$

where ε_{th} is the relative permittivity, V_m is the molar volume, and α is the ion polarizability.

The variations in the quality factor ($Q \times f$) of four components at different sintering temperatures are illustrated in Fig. 8 (b). As the sintering temperature increases, the $Q \times f$ values gradually rise to a peak and then decline. The trends of $Q \times f$ and bulk density remain largely consistent. At 1270 °C, the quality factor of all ceramic samples reached its maximum value.

Microwave dielectric loss is influenced by external factors such as material density and the presence of a second phase. In the current study, it has been determined that there is no second phase present in the $LnNbO_4$ ceramics, allowing us to exclude its influence. Furthermore, dielectric loss is significantly correlated with internal factors, including packing fraction (PF) and lattice vibrations. ABO_4 ceramics with a high packing fraction, which indicates a reduction in the internal atomic vibration interval, exhibit low microwave dielectric loss [23]. The packing fraction of a material can be calculated using Eq. (5) [24].

$$PF(\%)=\frac{V_{PI}}{V_{cell}}\times Z \quad (5)$$

where V_{PI} is the volume of stacked atoms, V_{cell} is the volume of the cell, Z

Table 3
Microwave dielectric properties of high-entropy $LnNbO_4$ ceramics sintered at 1270 °C.

sample	ST (°C)	ε_r	$Q \times f$ (GHz)	τ_f (ppm/°C)	α (Å^3)	α/V_m	PF (%)	$V_{Nb\text{-}O}$	reference
3RNO	1270	19.13	16190	1.75	17.2833	0.2102	60.85	4.2714	[16]
4RNO	1270	19.22	44920	−5.87	16.9575	0.2166	61.38	4.3248	[16]
5RNO	1270	19.48	47770	−13.50	16.7300	0.2233	61.81	4.4058	[16]
6RNO	1270	18.95	42600 (4)	−34.79 (3)	16.5067	0.2164 (6)	62.41	5.2878	this work
7RNO	1270	18.97	35200 (3)	−23.28 (7)	16.5071	0.2165 (2)	62.42	4.8630	this work
8RNO	1270	18.62	14000 (3)	−27.41 (2)	16.4888	0.2164 (3)	62.48	4.8798	this work
10RNO	1270	19.07	13000 (7)	−29.69 (5)	16.3300	0.2170 (4)	63.06	5.0226	this work

is the number of molecules in the cell, and R is the effective radius of the ion.

The results of the packing fraction calculations for the four RNO ceramics are presented in Table 3. As shown in Fig. 8 (b) and Table 3, the atomic packing fraction increases from 62.41 % for 6RNO to 63.06 % for 10RNO. However, the quality factor of the four components decreases, which can be attributed to the correlation between the Raman FWHM and damping behavior. The increase in the damping factor indicates a rise in ion disorder. Furthermore, the increase in intrinsic loss can be attributed to enhanced anharmonic vibrations [25,26]. The quality factor results from a competition between packing fraction and ion disorder [27]. As the configurational entropy of the 6RNO-10RNO ceramics increases (1.792R, 1.946R, 2.079R, 2.303R), the impact of ion disorder on the quality factor surpasses that of the packing fraction.

The temperature coefficients of resonant frequency (τ_f) in microwave dielectric ceramics are significantly influenced by their structural characteristics, including bond length and bond valence. Consequently, the ionic bond valence theory is frequently employed to investigate the thermal stability of microwave dielectric ceramics. The bond valence can be calculated using Eq. (6) and Eq. (7) [28].

$$V_i = \sum_j \nu_{ij} \tag{6}$$

$$\nu_{ij} = \exp\left(\frac{R_{ij} - d_{ij}}{b}\right) \tag{7}$$

where R_{ij} is the bond valence parameter [29], d_{ij} is the bond length between atoms i and j, and b is a constant (0.37 Å).

It has been shown that τ_f is related to bond valence; a decrease in bond valence results in a reduction of bond energy as well as the restoring force of the oxygen polyhedral tilt. This relationship is conducive to modulating the resonant frequency temperature coefficient of the ceramic material towards zero [30,31]. Table 3 presents the results of the calculation of the B-site bond valence ($V_{Nb\text{-}O}$). The B-site bond valence ($V_{Nb\text{-}O}$) ranges from 4.8630 (7RNO) to 5.2878 (6RNO), and the τ_f of the ceramics correspondingly decreases from −23.28 ppm/°C to −34.79 ppm/°C. The τ_f of all ceramic samples is inversely proportional to bond valence ($V_{Nb\text{-}O}$), and the test results align with the theoretical framework established in previous research [32].

4. Conclusions

This study reports the synthesis of four single-phase ultra-high-entropy ceramics: (La, Nd, Sm, Ho, Yb, Y)NbO_4 (6RNO), (La, Nd, Sm, Eu, Ho, Yb, Y)NbO_4 (7RNO), (La, Nd, Sm, Eu, Gd, Ho, Yb, Y)NbO_4 (8RNO), and (La, Nd, Sm, Eu, Gd, Ho, Yb, Y, Tm, Lu)NbO_4 (10RNO) using the solid-state method. All RNO ceramics were confirmed to possess a monoclinic fergusonite structure (space group $C2/c$) and exhibited optimal sintering characteristics and dielectric properties at 1270 °C, with well-developed grains and clear grain boundaries observed on the microstructure, and no porosity or microcracks were detected. Among them, the 7RNO ceramics sintered at 1270 °C demonstrated the best overall microwave dielectric properties, with a relative density of 95.43 %, $\varepsilon_r = 18.62$, $Q \times f = 35200$ GHz, and $\tau_f = -23.28$ ppm/°C. The results indicate that increasing configurational entropy enhances compositional homogeneity and stabilizes the single-phase monoclinic structure. However, the ionic disorder associated with high configurational entropy may lead to higher intrinsic dielectric losses, as evidenced by the lower $Q \times f$ values observed in 8RNO and 10RNO. The findings, when combined with previous high-entropy studies, suggest that while the high-entropy strategy is effective in stabilizing materials and can partially optimize dielectric properties, there exists an optimal level of configurational entropy for maximizing microwave dielectric performance.

CRediT authorship contribution statement

Xinrong Yang: Writing – original draft, Formal analysis, Data curation. **Deqin Chen:** Methodology, Investigation, Formal analysis, Data curation. **Guobin Zhu:** Writing – review & editing, Writing – original draft, Supervision, Data curation. **Siyu Xiong:** Validation, Software. **Xiaowei Zhu:** Supervision, Software. **Laijun Liu:** Resources, Project administration, Funding acquisition. **Chunchun Li:** Writing – review & editing, Supervision, Methodology, Conceptualization.

Declaration of competing interest

The authors declare that they have no known competing financial interests or personal relationships that could have appeared to influence the work reported in this paper.

Acknowledgments

The authors gratefully acknowledge the financial support from the Natural Science Foundation of China (No. 62061011) and the Science and Technology Plan of Guangxi (No. ZY22096019).

References

[1] H.M. Xiang, Y. Xing, F.Z. Dai, H.J. Wang, L. Su, L. Miao, G.J. Zhang, Y.G. Wang, X. W. Qi, L. Yao, H.L. Wang, B. Zhao, J.Q. Li, Y.C. Zhou, High-entropy ceramics: present status, challenges, and a look forward, J. Adv. Ceram. 10 (3) (2021) 1–57.
[2] H.Y. Li, Y. Zhou, Z.H. Liang, H.L. Ning, X. Fu, Z.H. Xu, T. Qiu, W. Xu, R.H. Yao, J. B. Peng, High-entropy oxides: advanced research on electrical properties, Coating. 11 (6) (2021) 628.
[3] C.M. Rost, E. Sachet, T. Borman, A. Moballegh, E.C. Dickey, D. Hou, J.L. Jones, S. Curtarolo, J.P. Maria, Entropy-stabilized oxides, Nat. Commun. 6 (2015) 8485–8492.
[4] L. Feng, W.G. Fahrenholtz, G.E. Hilmas, Y. Zhou, Synthesis of single-phase high-entropy carbide powders, Scripta Mater. 162 (2019) 90–93.
[5] L. Feng, W.G. Fahrenholtz, G.E. Hilmas, Processing of dense high-entropy boride ceramics, J. Eur. Ceram. Soc. 40 (12) (2020) 3815–3823.
[6] A. Salian, P. Sengupta, I.V. Aswath, A. Gowda, S. Mandal, A review on high entropy silicides and silicates: fundamental aspects, synthesis, properties, Int. J. Appl. Ceram. Technol. 20 (5) (2023) 2635–2660.
[7] X.Q. Chen, Y.Q. Wu, High-entropy transparent fluoride laser ceramics, J. Am. Ceram. Soc. 103 (2) (2020) 750–756.
[8] J. Chen, W.X. Liu, J.X. Liu, X.L. Zhang, M.Z. Yuan, Y.L. Zhao, J.J. Yan, M.Q. Hou, J. Y. Yan, M. Kunz, N. Tamura, H.Z. Zhang, Z.L. Yin, Stability and compressibility of cation-doped high-entropy oxide $MgCoNiCuZnO_5$, J. Phys. Chem. C 123 (29) (2019) 17735–17744.
[9] J. Liu, H. Liu, P.J. Chen, J.B. Hao, Microstructural characterization and corrosion behaviour of $AlCoCrFeNiTi_x$ high-entropy alloy coatings fabricated by laser cladding, Surf. Coat. Technol. 361 (15) (2019) 63–74.
[10] A.J. Wright, Q.Y. Wang, C.Y. Huang, A. Nieto, R.K. Chen, J. Luo, From high-entropy ceramics to compositionally-complex ceramics: a case study of fluorite oxides, J. Eur. Ceram. Soc. 40 (5) (2020) 2120–2129.
[11] H.C. Xiang, L. Yao, J.Q. Chen, A.H. Yang, H.T. Yang, L. Fang, Microwave dielectric high-entropy ceramic $Li(Gd_{0.2}Ho_{0.2}Er_{0.2}Yb_{0.2}Lu_{0.2})GeO_4$ with stable temperature coefficient for low-temperature cofired ceramic technologies, J. Mater. Sci. Technol. 93 (2021) 28–32.
[12] K. Liu, H.W. Zhang, C. Liu, J. Li, L. Shi, X.Y. Wang, D.N. Zhang, Crystal structure and microwave dielectric properties of $(Mg_{0.2}Ni_{0.2}Zn_{0.2}Co_{0.2}Mn_{0.2})_2SiO_4$-a novel high-entropy ceramic, Ceram. Int. 48 (16) (2022) 23307–23313.
[13] M.J. Xie, X. Li, Y.M. Lai, C. Qi, J. Yin, W.P. Gong, Y.X. Li, Q. Liu, C.S. Wu, Phase evolution and microwave dielectric properties of high-entropy spinel-type $(Mg_{0.2}Co_{0.2}Ni_{0.2}Li_{0.4}Zn_{0.2})Al_2O_4$ ceramics, J. Eur. Ceram. Soc. 44 (1) (2024) 284–292.
[14] T. Su, H.L. Chen, Z.Y. Wei, M.Y. Hao, X.D. Wang, Y.F. Liu, C. Ma, Y. Miao, F. Gao, Structure and microwave dielectric properties of Al^{3+}-doped $(Zn_{1/6}Ba_{1/6}Ca_{1/6}Sr_{1/6}La_{1/3})TiO_3$ high-entropy ceramics system, Ceram. Int. 50 (3PA) (2024) 5043–5051.
[15] H.R. Tian, X.H. Zhang, W. Du, Z.B. Feng, L.G. Wang, H.T. Wu, W.S. Xia, Structure characteristics and microwave/terahertz dielectric response of low-permittivity $(La_{0.2}Nd_{0.2}Sm_{0.2}Eu_{0.2}Gd_{0.2})_2Zr_3(MoO_4)_9$ high-entropy ceramics, Ceram. Int. 50 (4) (2024) 6403–6411.
[16] D.Q. Chen, N. Yan, X.F. Cao, F.R. Li, L.J. Liu, Q.H. Shen, H.F. Zhou, C.C. Li, Entropy regulation in $LaNbO_4$-based fergusonite to implement high-temperature phase transition and promising dielectric properties, J. Adv. Ceram. 12 (5) (2023) 1067–1080.
[17] P. Zhang, Y.J. Feng, Y. Li, W. Pan, P.A. Zong, M.Z. Huang, Y. Han, Z.S. Yang, H. Chen, Q.M. Gong, C.L. Wan, Thermal and mechanical properties of ferroelastic $RENbO_4$ (RE = Nd, Sm, Gd, Dy, Er, Yb) for thermal barrier coatings, Scripta Mater. 180 (2020) 51–56.

[18] Y.Q. Jia, Crystal radii and effective ionic radii of the rare earth ions, J. Solid State Chem. 95 (1) (1991) 184–187.
[19] H.C. Yang, S.R. Zhang, H.Y. Yang, Y. Yuan, E.Z. Li, Bond characteristics, vibrational spectrum and optimized microwave dielectric properties of chemically substituted $NdNbO_4$, Ceram. Int. 45 (14) (2019) 16940–16947.
[20] K.P.F. Siqueira, R.L. Moreira, A. Dias, Synthesis and crystal structure of lanthanide orthoniobates studied by vibrational spectroscopy, Chem. Mater. 22 (8) (2010) 2668–2674.
[21] J.W. Hou, Q. Chen, C. Gao, R.C. Dai, J.W. Zhang, Z.P. Wang, Z.M. Zhang, Z.J. Ding, Raman and luminescence studies on phase transition of $EuNbO_4$ under high pressure, J. Rare Earths 32 (9) (2014) 787–791.
[22] H. Sun, Y.F. Wang, Y.F. Liu, R.F. Wu, A.M. Chang, P.J. Zhao, B. Zhang, Enhanced thermal stability and broad temperature range in high-entropy $(La_{0.2}Ce_{0.2}Nd_{0.2}Sm_{0.2}Eu_{0.2})NbO_4$ ceramics, ACS Appl. Mater. Interfaces 16 (10) (2024) 12821–12832.
[23] G.B. Zhu, F.R. Li, D.Q. Chen, X.W. Zhu, S.Y. Xiong, H.X. Xiao, L.J. Liu, C.C. Li, Effect of raw material pretreatment and ionic radius on the preparation and microwave dielectric properties of Re_2TiO_5 ceramics, Ceram. Int. 50 (11PA) (2024) 19194–19201.
[24] Z.J. Qing, A. Liu, S.M. Duan, H.Y. Li, Y. Xue, Structure, chemical bonding characteristics and microwave dielectric properties of $Li_5Mg_3Ti_2O_9F$ ceramic with low sintering temperature, Ceram. Int. 50 (9PA) (2024) 15195–15201.
[25] B.H. Huang, T. Xia, F. Shang, G.H. Chen, A new BaB_2O_4 microwave dielectric ceramic for LTCC application, J. Eur. Ceram. Soc. 43 (14) (2023) 6107–6111.
[26] Y.X. Li, D.Y. Liang, X. Zhang, Z. Xiong, Z.J. Qing, S. Peng, B. Tang, F. Si, Z.X. Fang, F. Wang, T.T. Liao, J.J. Chen, A low-temperature firing and low-loss $SrBi_2TeO_7$ microwave dielectric ceramic for LTCC applications, J. Electron. Mater. 52 (2023) 7438–7466.
[27] G.B. Zhu, C.C. Li, S.Y. Xiong, X.W. Zhu, D.Q. Chen, H.B. Cui, L.J. Liu, Near-zero temperature coefficient of resonance frequency in rare-earth titanates via the phase transition strategy, ACS Appl. Mater. Interfaces. 16 (2024) 46473–46485.
[28] Y. Wang, B.B. Cao, M.A. Shi, W.S. Xia, H.T. Wu, Structure characteristics and microwave dielectric properties of novel $Re_2Ce_6O_{15}$ (Re = Y, Sm, Nd, La) ceramics, Ceram. Int. 49 (13) (2023) 21988–21993.
[29] N.E. Brese, M. O'Keeffe, Bond-valence parameters for solids, Acta Crystallogr. 47 (2) (1991) 192–197.
[30] E.S. Kim, B.S. Chun, R. Freer, R.J. Cernik, Effects of packing fraction and bond valence on microwave dielectric properties of $A^{2+}B^{6+}O_4$ (A^{2+}: Ca, Pb, Ba; B^{6+}: Mo, W) ceramics, J. Eur. Ceram. Soc. 30 (7) (2010) 1731–1736.
[31] M. Xiao, Q.Q. Gu, Z.Q. Zhou, P. Zhang, Study of the microwave dielectric properties of $(La_{1-x}Sm_x)NbO_4$ (x = 0-0.10) ceramics via bond valence and packing fraction, J. Am. Ceram. Soc. 100 (9) (2017) 3952–3960.
[32] H.S. Park, K.H. Yoon, E.S. Kim, Relationship between the bond valence and the temperature coefficient of the resonant frequency in the complex perovskite $(Pb_{1-x}Ca_x)[Fe_{0.5}(Nb_{1-y}Ta_y)_{0.5}]O_3$, J. Am. Ceram. Soc. 84 (1) (2001) 99–103.